

# New Computational Perspectives on Scattering and Transport in III/V Channel Materials

Z. Stanojević, M. Karner, F. Mitterbauer, C. Kernstock  
 Global TCAD Solutions GmbH., Landhausgasse 4/1a, 1010 Vienna, Austria  
 Email: {z.stanojevic|m.karner|f.mitterbauer|c.kernstock|h.demel}@globaltcad.com

## I. INTRODUCTION AND METHODOLOGY

III/V materials are considered good candidates for the replacement of silicon as the channel material due to their low effective mass. The combination of non-planar technology with III/V channel materials shows the most potential since it benefits from both superior material properties and good electrostatic control [1]. We took the opportunity to review the methodology for simulating III/V-channels and extend it to non-planar technology.

### A. Electronic structure and transport

The electronic structure is modeled using an anisotropic effective mass Hamiltonian with non-parabolic correction,

$$E_{\text{kin}}(1 + \alpha E_{\text{kin}}) = \frac{\hbar}{2} \mathbf{k} \cdot \mathbf{m}^{-1} \cdot \mathbf{k}, \quad (1)$$

for  $\Gamma$ , L, and X-valleys. This Hamiltonian was shown to be effective for the modeling of conduction band in III/V nanostructures [2, 3], as it correctly reproduces the hyperbolic dispersion relation at high energies. The non-parabolic correction is taken into account on three levels: (i) the confinement energies, (ii) the density of states, and (iii) the electron group velocity. The non-parabolic distortion is calculated for each subband individually accounting for the base kinetic energy due to confinement. To obtain the occupancy the Fermi-Dirac integrals need to be computed by numerical quadrature, due to the non-parabolic correction terms.

Transport is modeled on top of the subband structure using the linearized Boltzmann-transport-equation (LBTE),

$$\sum_{n', \mathbf{k}'} S_{n, n'}(\mathbf{k}, \mathbf{k}') \left[ \tau_{n, \xi}(E) \frac{\hbar k_{\xi}}{m_{n, \xi}} - \tau_{n', \xi}(E) \frac{\hbar k'_{\xi}}{m_{n', \xi}} \right] = \frac{\hbar k_{\xi}}{m_{n, \xi}}, \quad (2)$$

where an energy-dependent anisotropic relaxation time tensor  $\tau_{n, \xi}$  is used [4], thus avoiding the shortcomings of the momentum relaxation time approximation [5]. By solving the LBTE numerically, channel mobility and conductivity are obtained.

### B. Scattering models

In contrast to silicon, the most important scattering process in III/V semiconductors at room temperature is scattering by polar-optical phonons (POP). POP scattering differs from non-polar phonon scattering; unlike non-polar lattice vibrations, which interact with the electrons by altering the band structure through crystal deformation, polar phonons constitute oscillating electric dipoles. Hence, POP scattering constitutes an electrostatic perturbation, which is of long-range nature. It is unclear whether the bulk perturbation Hamiltonian for electron-POP interaction [6, 7] is still applicable as we deal with different materials with different dielectric properties. Also, smaller device feature sizes mean more pronounced

geometry and long-range effects. We thus propose an extension to the POP scattering model which takes the entire cross-section geometry into account, with the square modulus of the matrix element being

$$\langle |H_{n, n'; \mathbf{k}, \mathbf{k}'}|^2 \rangle = \frac{q_0^2 \hbar \omega \epsilon_0}{2L^{3-d}} \left( N + \frac{1}{2} \pm \frac{1}{2} \right) \int (\epsilon_{\mathbf{r}}^{\infty})^2 \left( \frac{1}{\epsilon_{\mathbf{r}}^{\infty}} - \frac{1}{\epsilon_{\mathbf{r}}^0} \right) \|\nabla U_{n, n'; \mathbf{k}, \mathbf{k}'}(\mathbf{r})\|^2 d^d r, \quad (3)$$

$$U_{n, n'; \mathbf{k}, \mathbf{k}'}(\mathbf{r}) = q_0 \int \psi_{n, \mathbf{k}}^*(\mathbf{r}') \psi_{n', \mathbf{k}'}(\mathbf{r}') G_{\mathbf{k}-\mathbf{k}'}^{\infty}(\mathbf{r}, \mathbf{r}') d^d r'. \quad (4)$$

$U_{n, n'; \mathbf{k}, \mathbf{k}'}(\mathbf{r})$  is the perturbation matrix element of a single point charge at  $\mathbf{r}$ , which is also used for Coulomb scattering. The approach is based on the high-frequency electrostatic Green's function  $G_{\mathbf{k}-\mathbf{k}'}^{\infty}(\mathbf{r}, \mathbf{r}')$ , which, when evaluated numerically from a discretized Poisson equation, takes into account geometry and spatial variation of the dielectric constant.

In addition to the POP scattering model, we employ our surface roughness scattering (SRS) model for non-planar devices [8] as well as non-polar acoustic, optical intra-valley, and inter-valley scattering models.

The entire modeling chain has been implemented within the VSP simulator [9], part of GTS Framework [10].

## II. SIMULATION AND RESULTS

As a simulation example we used the device architecture presented in [1], which consists of an  $\text{In}_{0.7}\text{Ga}_{0.3}\text{As}$  layer grown on top of a  $\text{In}_{0.52}\text{Al}_{0.48}\text{As}$  buffer, topped by an InP etch stop. The fins are cut out from the InGaAs/InP layers and  $\text{TaSiO}_x$  is deposited isotropically onto the free surfaces.

We first analyzed the long-channel properties of the InGaAs FinFET, by computing the transconductance curve of a 40  $\mu\text{m}$  long gated fin. The transconductance, shown in Fig. 1, is seen to be dominated by POP and surface-roughness. The process limited mobilities in Fig. 2 give a more detailed picture: POP limits the mobility in the low-density regime, while scattering off the rough  $\text{TaSiO}_x$  interface limits mobility at higher densities.

To examine the properties of a realistic InGaAs FinFET, we combined the electronic structure/transport calculation with the device simulator Minimos-NT [11] using *self-consistent quantum correction*, as shown in Fig. 3. The coupling procedure between the two simulators is depicted in Fig. 4. The thus obtained characteristic and parameters are shown in Fig. 5.

We have demonstrated a framework for simulating novel III/V-based non-planar transistor architectures. The framework is based on physical modeling of electronic structure, scattering, and transport. A combination with a 3D device simulator allows to leverage the benefits of physical modeling for the simulation of entire devices.

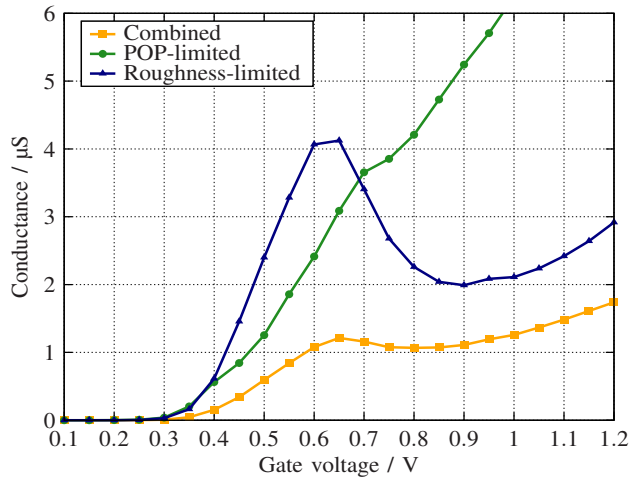


Fig. 1. Transconductance curve for a 40µm long gated fin;  $\Pi$ -gated fin the has a rectangular shape, 10 nm wide, 20 nm high with a 1 nm InP-layer on top, and is surrounded by 2 nm-layer of TaSiO<sub>x</sub> and a metal gate. POP scattering and SRS dominate transport in the channel. Starting from 0.6 V conductance becomes severely degraded by SRS.

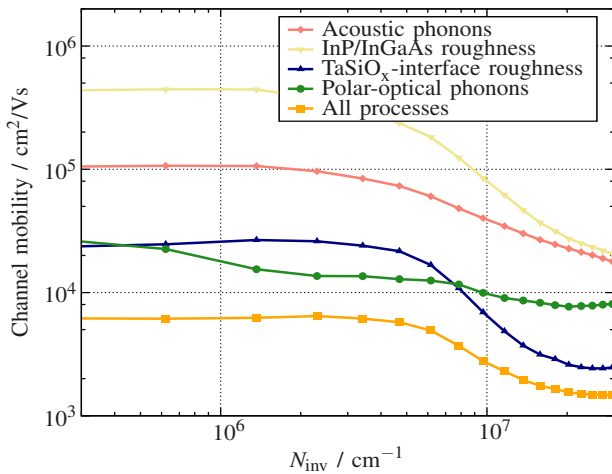


Fig. 2. Electron mobility plotted against the inversion density in the fin; POP scattering and SRS clearly dominate electron transport with SRS on the TaSiO<sub>x</sub>-interfaces being far more important than SRS on InGaAs/InP-interfaces.

#### REFERENCES

- [1] M. Radosavljevic *et al.*, *Electron Devices Meeting (IEDM), 2010 IEEE International* (2010), pp. 6.1.1–6.1.4.
- [2] D. Lizzit *et al.*, *Electron Devices, IEEE Transactions on* **61**, 2027 (2014).
- [3] O. Baumgartner *et al.*, *Book of Abstracts of the 16th International Workshop on Computational Electronics (IWCE)* (2013), pp. 86–87.
- [4] Z. Stanojević *et al.*, *Solid-State Electronics* (2015), in press.
- [5] Z. Stanojevic *et al.*, *SISPAD* (2014), pp. 181–184.
- [6] H. Fröhlich, *Proceedings of the Royal Society A* (1937), Vol. 160, pp. 230–241.
- [7] B. Ridley, *Quantum Processes in Semiconductors* (Oxford University Press, 2013).
- [8] Z. Stanojevic *et al.*, *Intl. Electron Device Meeting* (2013), pp. 332–335.
- [9] O. Baumgartner *et al.*, *J. Comput. Electron.* **12**, 701 (2013).
- [10] GTS Framework, <http://www.globalcad.com/framework>.
- [11] Minimos-NT, <http://www.globalcad.com/minimos-nt>.

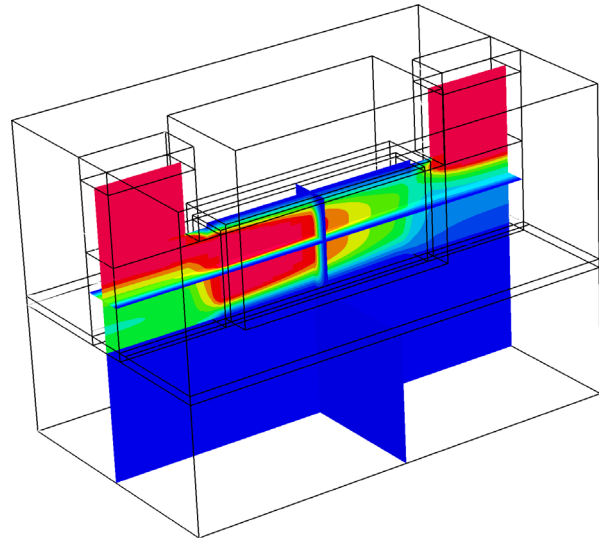


Fig. 3. Electron concentration in an InGaAs FinFET at  $V_G = 1$  V and  $V_{DS} = 0.1$  V; fin width and height are 10 nm and 20 nm, respectively, gate length is 50 nm; the confinement effect due to self-consistent quantum correction is clearly visible.

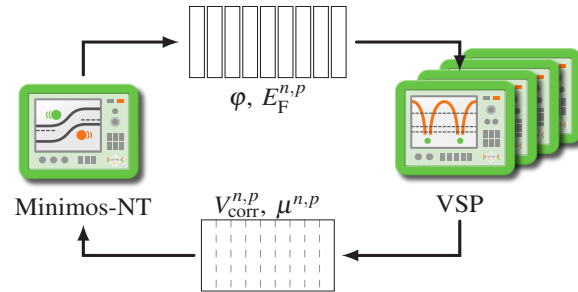


Fig. 4. Schematic overview of the coupling between Minimos-NT and VSP; The simulation domain is decomposed into slices on each of which Minimos-NT invokes a VSP instance (in parallel) and passes the electrostatic potential along with the quasi-Fermi-energies. VSP returns the quantum correction potential and the mobility for the slice which are interpolated back onto the original 3D simulation domain.

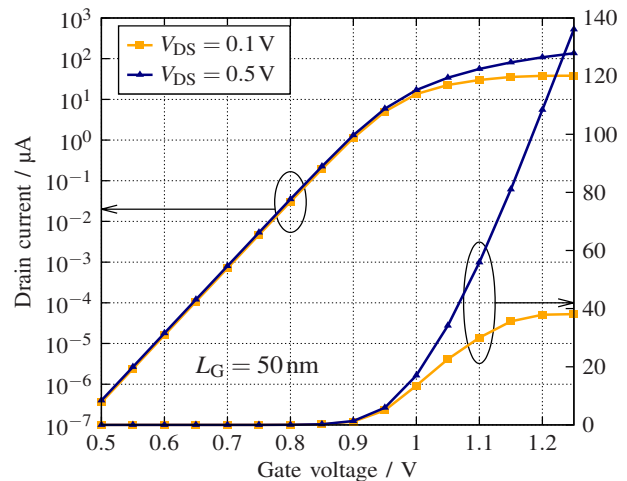


Fig. 5. Transfer characteristic of the InGaAs FinFET shown in Fig. 3 at 0.1 V and 0.5 V drain bias; the FinFET shows excellent electrostatic control of the channel with a subthreshold slope of 61.5 mV/dec and a DIBL of 9.19 mV/V.